

Photocatalytic water splitting on Au/TiO₂ nanocomposites synthesized through various routes: Enhancement in photocatalytic activity due to SPR effect

Sadhana S. Rayalu^{a,b,*}, Deepa Jose^{c,1}, Meenal V. Joshi^{a,b,1}, Priti A. Mangrulkar^{a,b}, Khadga Shrestha^c, Kenneth Klabunde^c

^a CSIR-Network Institute of Sustainable Energy (CSIR-NISE), India

^b Environmental Materials Division, CSIR-National Environmental Engineering Research Institute (CSIR-NEERI), Nagpur 440 020, India

^c Department of Chemistry, Kansas State University, Manhattan, KS 66506, United States

ARTICLE INFO

Article history:

Received 22 January 2013

Received in revised form 8 May 2013

Accepted 22 May 2013

Available online 12 June 2013

Keywords:

Plasmonic

Photodeposition

Photocatalytic hydrogen

Visible light

Gold nanoparticles

ABSTRACT

In the present investigation, Au/TiO₂ nanocomposites were prepared by in situ, photodeposition (PD) and SMAD method. The synthesized photocatalysts were evaluated for their photocatalytic activity in hydrogen generation. The hydrogen evolution rate was observed to be 1200 $\mu\text{mol h}^{-1}$, 920 $\mu\text{mol h}^{-1}$ and 1600 $\mu\text{mol h}^{-1}$ for in situ, photodeposition (PD) and SMAD, respectively under UV–vis light illumination. However, under purely visible light illumination the highest hydrogen evolution of 32.4 $\mu\text{mol h}^{-1}$ was observed in case of Au/TiO₂ prepared by PD followed by SMAD (6.9 $\mu\text{mol h}^{-1}$). The significantly high photocatalytic activity as demonstrated by Au/TiO₂ synthesized by photodeposition method under purely visible light irradiation proves the potential of photocatalyst in efficient solar energy conversion. The poly disperse particles of AuNPs on TiO₂ by photodeposition method enhances plasmonic effects. The catalyst was thoroughly characterized by powdered X-ray diffraction, UV–vis DRS and TEM for understanding the plasmonic properties. TEM images further substantiated the deposition of gold on TiO₂ matrix of heterogeneous particle size with an average size of 8–10 nm (smaller particles) and 53–70 nm (bigger particles). The photodeposition of AuNPs on different titania supports was also studied.

© 2013 Elsevier B.V. All rights reserved.

1. Introduction

Solar energy is a compelling solution to our need for clean and abundant source of energy in future. One of the major reasons for its low utilization is its diffuse and intermittent availability. It is therefore imperative to address the issue of solar energy conservation systems, in specific, solar fuels including hydrogen. Semiconductor based water splitting reaction using solar energy for hydrogen generation is by far most studied reaction. Absorption of light energy to convert it into chemical energy is a tough target till date. It is envisaged that exploring the options of surface plasmon resonance for better light absorption, increased charge separation and suppression of electrons and holes may significantly improve the hydrogen generation [1]. Chemical properties of metals are based on their

electronic motion and these electronic motions invariably depend on space available. This means that chemical properties of metal are size and shape dependent and if the size of the atom is reduced below original dimension then its properties become shape and size sensitive [2]. In case of noble metals if the size is reduced below its electron mean path (distance between the scattering collision and lattice centre) it induces the property of visible and near UV light absorption with consequent coherent oscillation of electrons on particle surface (surface plasmon resonance-SPR). The phenomena of SPR is well reported and briefly stating it implies the collective oscillation of the valence electrons of the noble metal under visible light irradiation which consequently leads to enhanced electric field. The SPR effect can be instrumental in increasing the energy intensity of the photogenerated charge carriers thereby increasing the photocatalytic activity.

Metals like platinum [3], gold [4], silver [5,6] and copper in nano form are known for their resonance under illumination and these metal nanoparticles have applications in various fields such as catalysis, photocatalysis [7], bio-sensors [8] and also in optical applications [9]. Inherent drawbacks of TiO₂ semiconductors are rapid electron-hole recombination and light absorption in ultra-violet region. These drawbacks can be overcome by coupling

* Corresponding author at: Environmental Materials Division, CSIR-National Environmental Engineering Research Institute (CSIR-NEERI), Nagpur-440020, India. Tel.: +91 7122247828; fax: +91 7122249900.

E-mail addresses: s.rayalu@neeri.res.in, rayaluss@gmail.com (S.S. Rayalu), priti1804@gmail.com (P.A. Mangrulkar).

¹ These authors have contributed equally.

semiconductor with plasmonic metal nanoparticles. These plasmonic metal nanoparticles are expected not only to improve visible light absorption but also minimize electron–hole recombination reaction.

Activity of nanoparticles is based on three factors including (i) size of nanoparticles wherein it is reported that gold nanoparticles with particle size below 20 nm are catalytically more active [10,11], (ii) choice of support wherein it is reported that TiO_2 , Fe_2O_3 , Ce_2O_3 and ZrO_2 are the most preferred supports [12,13] and (iii) method of synthesis which has a vital implication on the size of metal nanoparticles. There are many reports available for synthesis of gold nanoparticles via different synthesis routes such as Redmond et al. synthesized array of gold nanoparticles of average radius size of 37.5 nm by using electron beam lithography on indium tin oxide (ITO) coated glass electrodes [14]. Isaac Ojea-Jime'nez et al. synthesized small gold nanoparticles using sodium citrate reduction and heavy water, with consequent reduction in the size of gold nanoparticles around 5.3 ± 1.1 nm [15]. Wang et al. reported the synthesis of gold clusters on TiO_2 support and concluded that gold clusters smaller in size exhibit higher catalytic property [16]. There are various other methods reported for gold nanoparticle synthesis [17–21]. Au/TiO_2 has been used for various catalytic applications. Haruta et al. used Au/TiO_2 as a catalyst for selective CO oxidation [22,23]. Recently, Alvaro reported visible light activity of gold nanoparticles supported on mesoporous titania for decontamination of chemical warfare agent pinacol methylphosphonofluoridate (soman) [24]. Dozzi investigated photocatalytic oxidation of formic acid, azo dye Acid Red-1 and hydrogen peroxide generation via oxygen reduction by Au nanoparticles deposited titania under visible light irradiation [25]. Kowalska deposited Au nanoparticles onto 15 different commercial titania and evaluated them for photocatalytic activity by photo oxidation of acetic acid and 2-propanol under visible light illumination [26]. It is evident from the literature that Au/TiO_2 has been extensively used as an oxidative photocatalyst with very few reports available on water splitting [6,27,28].

With this background, we synthesized Au/TiO_2 , Pt/TiO_2 and Cu/TiO_2 nanocomposites by photodeposition (PD) route for photocatalytic hydrogen generation. PD route is less energy intensive and directly deposits gold nanoparticles on TiO_2 surface thus eliminating the need of high temperature calcination step [29]. The synthesized nanocomposites were evaluated for sacrificial donor assisted photocatalytic water splitting reaction. Au/TiO_2 showed better photoactivity as compared to Pt/TiO_2 and Cu/TiO_2 and therefore Au was further deposited on three different titania supports such as Commercial Degussa P-25, Anatase (commercial) and Anatase synthesized by aerogel method. $\text{Au/TiO}_2(\text{P-25})$ showed remarkable increase in photocatalytic activity as compared to others and was therefore investigated in detail for studying various other parameters like effect of illumination source, Au concentration, etc. The role of SPR and the mechanistic aspects have also been discussed in this paper.

2. Experimental

2.1. Methods

Two types of TiO_2 phases such as Anatase (99.9%, Alfa Aesar) and P-25 (Degussa) along with gold chloride, platinum chloride, copper chloride and ethanol were procured from Sigma Aldrich. All the chemicals and reagents were used as such for synthesis and evaluations without any further purification.

2.2. Synthesis of M/TiO_2 ($M = \text{Au/Pt/Cu}$) by photodeposition (PD)

Photodeposition (PD) of metal (Au/Pt/Cu) onto TiO_2 matrix was carried out in a borosilicate glass reactor 500 mL capacity equipped

with outer glass jacket. Pre-weighed quantity of TiO_2 (Anatase/P-25/Aerogel) was suspended in 200 mL of de-ionized water and placed in a PD reactor. The reaction vessel was kept under inert atmosphere (N_2) for 30 min prior to addition of 2–4% w/w metal salt solution in reaction vessel. Ten mL of ethanol was added to the reactor and reaction vessel was illuminated with UV–visible source of tungsten and xenon lamps for 4 h under constant stirring. During illumination sample was shielded from heat by circulation of cold water. After completion of reaction, TiO_2 /metal nanocomposite was centrifuged, suspended in ethanol and dried in vacuum oven at 60°C . Gold chloride, platinum chloride and copper chloride were used as metal precursors for Au, Pt and Cu deposition respectively.

2.3. Synthesis of Au/TiO_2 by SMAD

Pre weighed quantity of Au and TiO_2 (60 mg Au + 2960 mg TiO_2) were loaded in a crucible and placed at the bottom of reactor. The reactor was evacuated in the presence of liquid nitrogen and heated resistively to achieve condensation of Au atom with solvent molecules. After completion of reaction the reactor was brought to the room temperature under Ar atmosphere. On cooling Au–solvent colloid comes in contact with TiO_2 , this mixture was then stirred for 2 h in Ar atmosphere, recovered and vacuum dried [30]. The SMAD process has an edge over other methods of synthesis of nanoparticles because of reproducibility, no formation of byproducts and scalability.

2.4. Instrumentation

Gold deposition on TiO_2 was analyzed by Powdered XRD at Scintag-XDS-2000 spectrometer with $\text{Cu K}\alpha$ radiation (applied voltage = 40 kV and current = 40 mA). Brunauer–Emmet–Teller (BET) measurements of surface area and pore size distribution of TiO_2 and Au/TiO_2 nanocomposites were determined using a Quantachrome NOVA 1200 N_2 gas adsorption/desorption analyzer at liquid nitrogen temperature. Light absorption range was determined by UV–visible diffuse reflectance spectra analyzed on Cary 500 scan UV–visible–NIR spectrophotometer working in air at room temperature over the range from 200 nm to 800 nm. Transmission electron microscopic images were recorded at Phillips CM100 electron microscope operating at 100 kV.

2.5. Photocatalytic water splitting experiments

2.5.1. Rapid screening method

Photocatalytic water splitting experiments were carried out in 40 mL glass vial under UV–visible light. In a typical experiment, 15 mg of Au/TiO_2 nanocomposite, 19 mL water and 1 mL ethanol were taken in a 40 mL glass vial and closed with screw cap. Vial was evacuated by applying vacuum in order to remove any air present in the head space. The reaction mixture was illuminated for 2 h with tungsten lamp. The headspace gas was injected into the GC and analyzed for the hydrogen.

2.5.2. Online photocatalytic evaluations

The photocatalytic experiments were carried out in a glass enclosed reaction chamber with a quartz inner radiation reaction vessel. The glass chamber was connected to a gas circulation evacuation and water cooling system. In a typical experiment, 100–250 mg catalyst, 322 mL distilled water and 18 mL ethanol were taken in the glass reactor with a magnetic stir bar. The reaction mixture was evacuated and filled with Ar five times to remove all the dissolved gases. This was followed by irradiation using a 450 W high pressure Hg lamp via a quartz tube. Water at 20°C was circulated continuously through the outer walls of the reactor and the quartz vessel to make sure that the temperature of the reaction

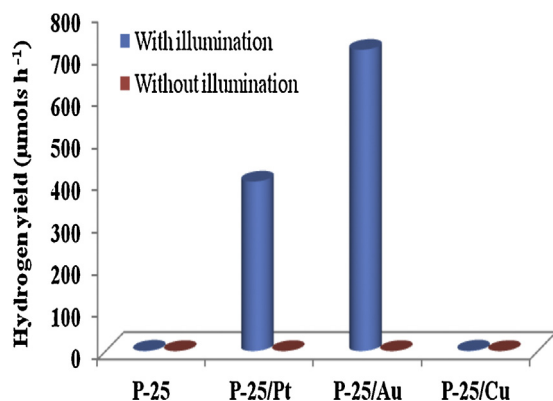


Fig. 1. Rapid screening of M (M = Au, Pt, Cu)/TiO₂(P-25) by photodeposition method (water:ethanol = 20:1, photocatalyst dose = 15 mg and time = 2 h).

mixture did not exceed 35 °C [31]. The activity of these catalysts for water splitting was investigated for 10 h irradiation period, using a fresh catalyst each time. Two molar NaNO₂ solution was used as a filter to cut off UV radiation in our visible studies. H₂ production was monitored using an online GC system (GOW-MAC 580 model) employing an All Tech molecular 80/100 sieve 5A column with Argon as the carrier gas and a thermal conductivity detector.

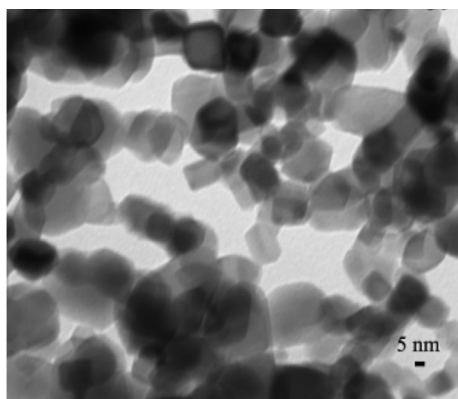
3. Results and discussion

3.1. Photocatalytic activity of metal/TiO₂ nanocomposite

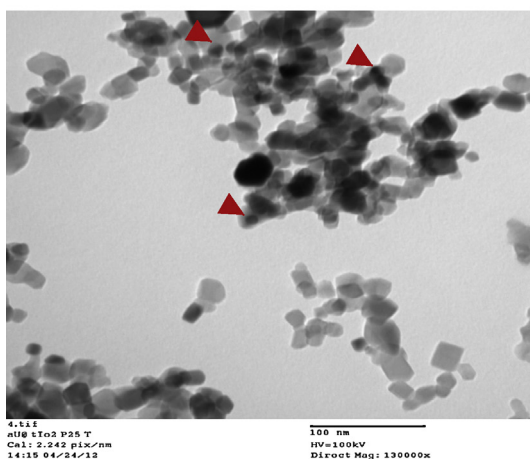
3.1.1. Screening of metal/TiO₂ nanocomposite by rapid screening method

Au/TiO₂(P-25), Pt/TiO₂(P-25) and Cu/TiO₂(P-25) synthesized by PD method along with TiO₂(P-25) as such were evaluated for ethanol assisted photocatalytic water splitting reaction under UV–visible irradiation. A parallel set of experiments were carried out without illumination. No hydrogen evolution was observed in case of samples without illumination. Fig. 1 shows the hydrogen evolution of M(Au, Pt, Cu)/TiO₂(P-25) nanocomposite by PD method. Hydrogen evolution rate of 16 mL h^{−1} was observed for Au/TiO₂(P-25). The hydrogen evolution rate was almost 1.8 times higher as compared to Pt/TiO₂(P-25). However Cu/TiO₂(P-25) has not shown any significant hydrogen generation. Therefore, further studies were restricted to Au/TiO₂(P-25) for further investigations.

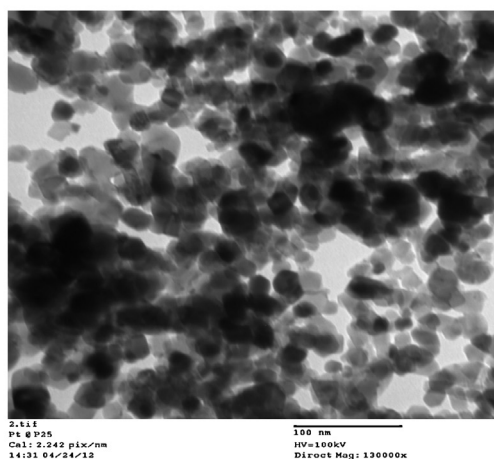
Bright field TEM images (Fig. 2) in case of Au/TiO₂(P-25) (Fig. 2b) has shown isolated gold particle deposition onto the semiconductor matrix with an average particle size ranging from 8–10 nm (small particles) to 53–70 nm (bigger particles). However, in case of Pt/TiO₂(P-25) (Fig. 2c) although metal deposition seems to be uniform, but it is in the form of agglomerates which may lower the photocatalytic activity in addition to the SPR effect. This agglomeration probably affects the photocatalytic activity of the composite.



(a) TiO₂(P-25)



b) Au/TiO₂ (4%w/w)



c) Pt/TiO₂ (4%w/w)

Fig. 2. Bright field TEM images of (a) TiO₂(P-25), (b) Au/TiO₂(P-25) and (c) Pt/TiO₂(P-25).

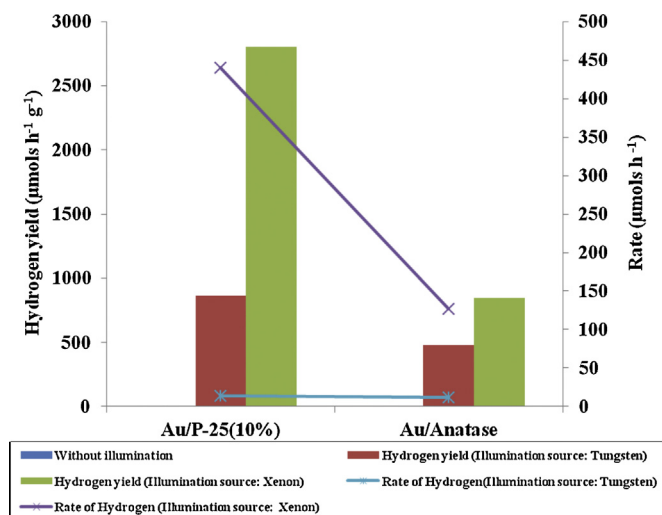
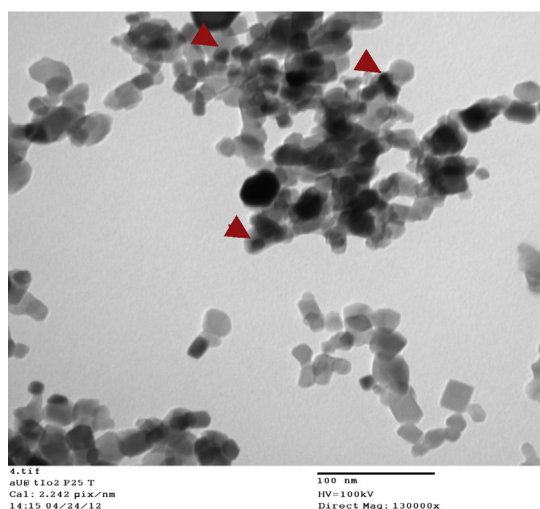


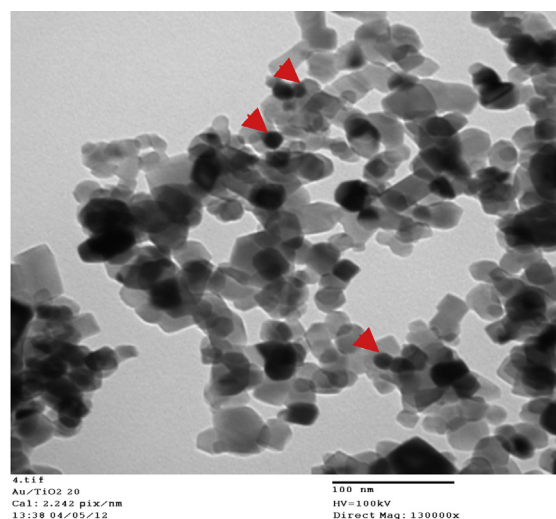
Fig. 3. Effect of illumination source on synthesis of $\text{Au/TiO}_2(\text{P-25})$ and $\text{Au/TiO}_2(\text{anatase})$. (water:ethanol = 322:18, photocatalyst dose = 150 mg and time duration = 5 h).

It is therefore required to further optimize the conditions rigorously in order to exploit the role of metals (Pt & Cu) as co-catalysts and their SPR effect.

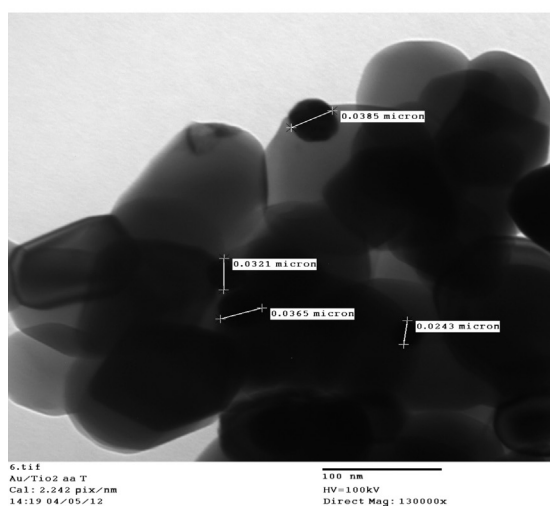
3.1.1.1. Effect of illumination source on PD of Au/TiO_2 . The effect of illumination source on photodeposition of $\text{Au/TiO}_2(\text{P-25})$ and $\text{Au/TiO}_2(\text{anatase})$ was investigated by varying the illumination source (tungsten and xenon lamps) during photodeposition. A parallel set of experiments were carried out without illumination. No hydrogen evolution was observed in case of samples without illumination. Fig. 3 shows the hydrogen yield obtained under different illumination conditions. The hydrogen yield to the tune of about $2802 \mu\text{mol h}^{-1} \text{g}^{-1}$ and hydrogen evolution rate of $440 \mu\text{mol h}^{-1}$ was observed for $\text{Au/TiO}_2(\text{P-25})$ nanocomposites synthesized by xenon lamp irradiation (1000 W). However, $\text{Au/TiO}_2(\text{P-25})$ sample synthesized using tungsten source (400 W) shows lower photoactivity with hydrogen evolution rate of $86.4 \mu\text{mol h}^{-1}$ and hydrogen yield of $864 \mu\text{mol h}^{-1} \text{g}^{-1}$. A similar trend was observed in case of $\text{Au/TiO}_2(\text{anatase})$. It can therefore be inferred that illumination using xenon lamp of 1000 W proved to be better illumination source.



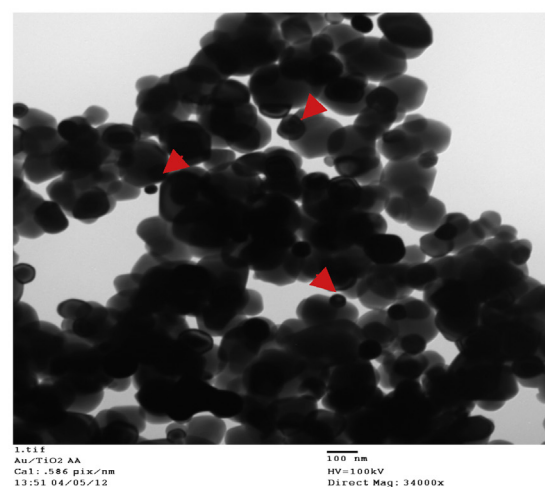
a) $\text{Au/TiO}_2(\text{P-25})$ (Tungsten)



b) $\text{Au/TiO}_2(\text{P-25})$ (Xenon)



c) $\text{Au/TiO}_2(\text{anatase})$ (Tungsten)



d) $\text{Au/TiO}_2(\text{anatase})$ (Tungsten)

Fig. 4. Bright field TEM images of (a) $\text{Au/TiO}_2(\text{P-25})$ (tungsten) (b) $\text{Au/TiO}_2(\text{P-25})$ (xenon), (c) $\text{Au/TiO}_2(\text{anatase})$ (tungsten) and (d) $\text{Au/TiO}_2(\text{anatase})$ (xenon).

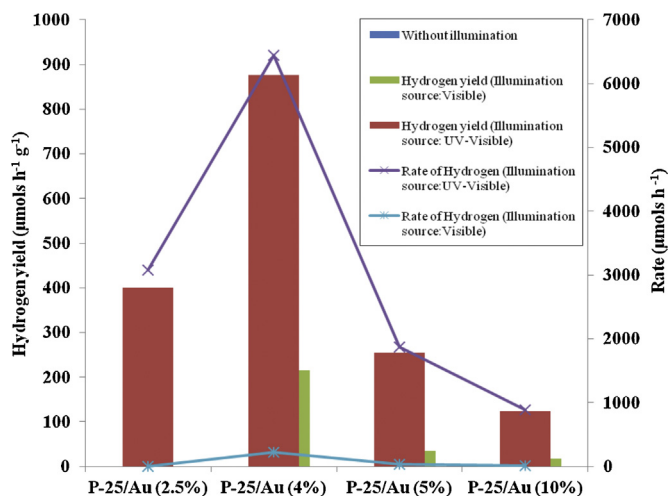


Fig. 5. Hydrogen evolution by varying of Au concentration on $\text{TiO}_2(\text{P-25})$. (water:ethanol = 322:18, photocatalyst dose = 150 mg and time duration = 5 h.)

Fig. 4 shows the bright field TEM images of $\text{Au}/\text{TiO}_2(\text{P-25})$ and $\text{Au}/\text{TiO}_2(\text{anatase})$ synthesized by tungsten and xenon source. From the figure it is clear that the source of illumination has direct effect on the formation of gold nanoparticles. Gold nanoparticles have a bigger particle size of about 60 nm when illuminated with tungsten lamp and have average particle size of 10–12 nm when illuminated with xenon light for $\text{Au}/\text{TiO}_2(\text{P-25})$. This finding corroborates with that reported by Scaniano et al. wherein particle size of gold by PD (in the presence of organic donors) reduced with increasing light intensity [32]. This supports the findings of our research work as well wherein bigger size AuNPs were observed for tungsten lamp of 400 W and smaller sized AuNPs were observed for xenon lamp (1000 W). Kowalska (2012) reported that Au nanoparticles formed in spherical/hemispherical shape shows better photoactivity as compared with rod shaped [33]. In the present work, the particles were spherical for AuNPs deposited by PD method. Thus, these two factors may be responsible for enhanced activity of $\text{Au}/\text{TiO}_2(\text{P-25})$ synthesized by PD method using xenon light.

3.1.1.2. Effect of variation of Au concentration on the activity of synthesized photocatalysts. Based on the above observation, Au concentration was varied for its photodeposition on titania using xenon light. The variation of concentration of Au is the most important parameter in order to optimize the synthesis for better photocatalytic activity. The concentration of gold in solution was varied from 2.5% to 10% w/w with respect to TiO_2 . Fig. 5 shows the effect of Au concentration variation on the activity of synthesized nanocomposites. $\text{Au}/\text{TiO}_2(\text{P-25})$ shows hydrogen evolution rate and yield of $440 \mu\text{mols h}^{-1}$ and $2802 \mu\text{mols h}^{-1} \text{ g}^{-1}$ initial gold concentration of 2.5% w/w.

The rate and yield increased by a factor of 2.09 and 4.31 on increasing the concentration to 4%. Further increase in concentration to 5% resulted in significant decline in activity with continual decline on further increase in concentration. These results are consistent with the finding reported by Anpo et al. Thus, Au synthesized with initial gold concentration of 4% w/w appears to be optimal concentration for synthesis of $\text{Au}/\text{TiO}_2(\text{P-25})$ by PD method. Higher hydrogen rate and yield both for UV-visible and visible radiations of $920 \mu\text{mols h}^{-1}$ and $32.4 \mu\text{mols h}^{-1}$, respectively illustrates combined effect of AuNP as co-catalyst and as a visible light harvester. It may thus be inferred that lower concentration of metal does not interrupt the light path of incident radiation (4% w/w), however increase in metal loading (5% and 10% w/w) has a consequent effect of metal acting as a half mirror which starts reflecting the amount of incident radiations [34]. This affects the overall absorption of light by metal-semiconductor composites and the catalytic activity of this composite.

Fig. 6 shows the TEM images of Au/TiO_2 nanocomposite synthesis with 5% and 10% initial gold concentration. From the figure it is apparent that increasing Au concentration resulted in covering of the entire surface of semi-conductor with AuNPs resulting in decrease in the photoresponse of the nanocomposite.

3.1.1.3. Effect of TiO_2 supports on the activity of synthesized photocatalysts. Three different types of TiO_2 such as P-25 (75% Anatase and 25% rutile), Anatase commercial ($\text{TiO}_2(\text{anatase})$) and aerogel (anatase) ($\text{TiO}_2(\text{aerogel})$) were used for Au photodeposition and then evaluated for photocatalytic hydrogen generation (Table 1). The

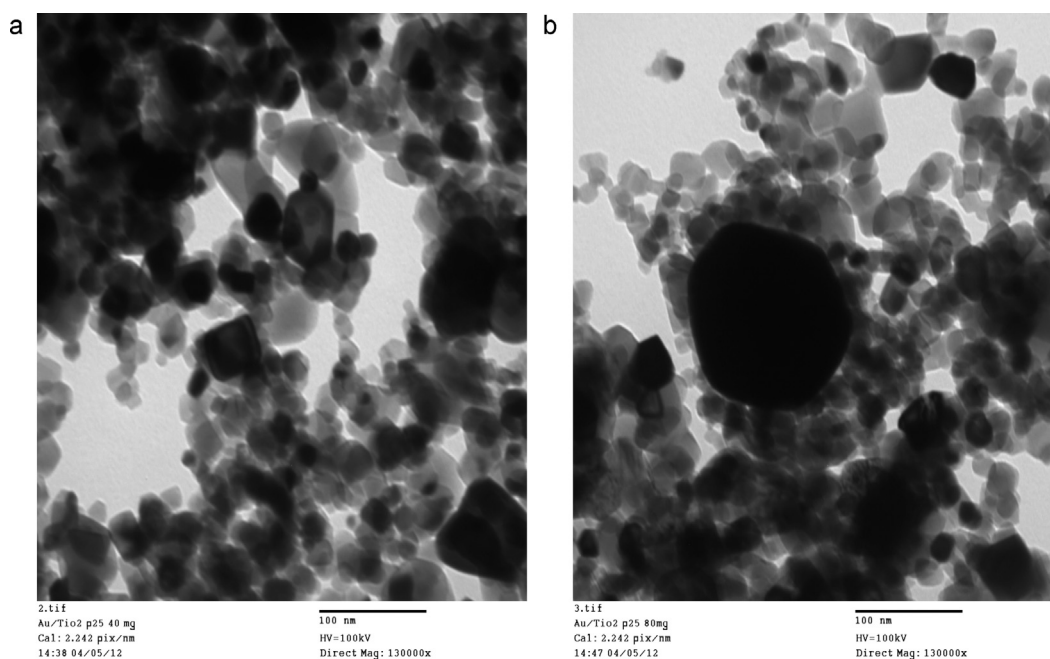


Fig. 6. Bright field TEM images of $\text{Au}/\text{TiO}_2(\text{P-25})$ (xenon) (a) Au (5%w/w)/ $\text{TiO}_2(\text{P-25})$ and (b) Au (10% w/w)/ $\text{TiO}_2(\text{P-25})$.

Table 1
Hydrogen generation in UV–visible and visible light irradiation by different titania.

Catalyst	Hydrogen yield ($\mu\text{mols h}^{-1}$)				
	Dark	UV-visible		Visible	
		$\mu\text{mols h}^{-1}$	$\mu\text{mols h}^{-1} \text{ g}^{-1}$	$\mu\text{mols h}^{-1}$	$\mu\text{mols h}^{-1} \text{ g}^{-1}$
TiO ₂ (P-25)	0	90	361	1.9	7.4
TiO ₂ (anatase)	0	1.7	6.6	ND	ND
TiO ₂ (aerogel)	0	18	120	ND	ND
Au/TiO ₂ (P-25)	0	920	6133	32.4	215
Au/TiO ₂ (anatase)	0	127	846	ND	ND
Au/TiO ₂ (aerogel)	0	460	4705	ND	ND

Photocatalytic water splitting on Au/TiO₂ nanocomposites synthesized through various routes: enhancement in photocatalytic activity due to SPR effect.

yield of hydrogen was observed to be higher in case of Au/TiO₂(P-25) photocatalyst under UV–visible and visible light illumination as mentioned in earlier section compared to Au deposited on other TiO₂ such as TiO₂(anatase) commercial (hydrogen yield to the tune of about $846 \mu\text{mols h}^{-1} \text{ g}^{-1}$ under UV–visible illumination with negligible evolution in visible light) and Au/TiO₂(aerogel) (hydrogen yield to the tune of about $4705 \mu\text{mols h}^{-1} \text{ g}^{-1}$ under UV–visible illumination with negligible evolution in visible light). There could be two possibilities (i) photodeposited plasmonic Au nanoparticles absorbs visible light around 540 nm and P-25 being partially visible active due to rutile quotient also absorbs visible light and therefore this synergy enhances overall activity of this photocatalyst in UV–visible and visible light illumination and (ii) Au nanoparticles of smaller particle size act as a co-catalyst and enhances the photoactivity where as particles with bigger particle size harvest visible light.

It is reported that anatase phase of TiO₂ is photocatalytically more active as compared to other phases such as amorphous TiO₂, rutile and brookite [35]. Our experimental data supports that the activity of anatase–rutile in definite ratio (75% anatase and 25% rutile) is higher than anatase alone. This also corroborates with the findings of Tsukamoto, wherein high catalytic activity in Au/rutile/anatase composite with Au particle size smaller than 5 nm has been reported. Higher activity is due to position of Au nanoparticle on interface of anatase/rutile TiO₂ which acts as the active site for reaction. It is reported that visible light promoted plasmon in Au nanoparticle located on the interface

of rutile/anatase of TiO₂ and the activated Au injected electron to the conduction band of rutile and then to the anatase TiO₂ [36].

Au/TiO₂(P-25) appears to be the most performing photocatalyst in UV–visible light illumination with hydrogen evolution rate of $920 \mu\text{mols h}^{-1}$ and hydrogen yield of $6133 \mu\text{mols h}^{-1} \text{ g}^{-1}$ followed by Au/TiO₂(aerogel) and Au/TiO₂(anatase). This may be attributed to the transfer of electron from anatase of TiO₂(P-25) to rutile of TiO₂(P-25) and thereafter its transfer to AuNP leading to delay in recombination reaction with consequent increase in hydrogen generation which is not the case in TiO₂(anatase). Amongst TiO₂(anatase) and TiO₂(aerogel), (TiO₂ being in anatase phase in both cases) the latter seems to be performing well which may be attributed to higher surface area of TiO₂(aerogel) ($102 \text{ m}^2 \text{ g}^{-1}$) as compared to TiO₂(anatase) ($13 \text{ m}^2 \text{ g}^{-1}$) and particle size of 0.1–0.2 μm in case of TiO₂(anatase) as compared to 10–15 nm for TiO₂(aerogel). Similar trend was observed in case of visible light irradiation wherein the hydrogen evolution rate was $32.4 \mu\text{mols h}^{-1}$ for Au/TiO₂(P-25) which was not shown by any other photocatalysts.

Fig. 7 shows bright field TEM images of (a) Au/TiO₂(aerogel) (b) Au/TiO₂(anatase). From the figure it is observed that, in case of Au/TiO₂(aerogel) there are clusters of Au nanoparticles and these clusters are localized near some particles restricting uniform dispersion of metal nanoparticles. For Au/TiO₂(anatase), bigger nanoparticles were present on TiO₂ surface almost covering the surface of the TiO₂(anatase) impeding the synergy of TiO₂–metal nanoparticles.

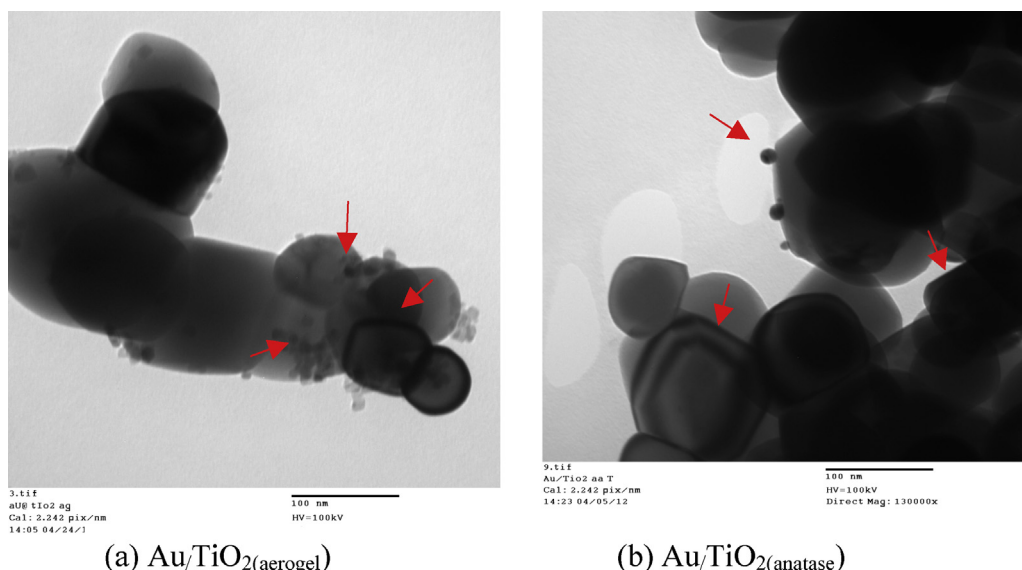


Fig. 7. Bright field TEM images of (a) Au/TiO₂(aerogel) (b) Au/TiO₂(anatase).

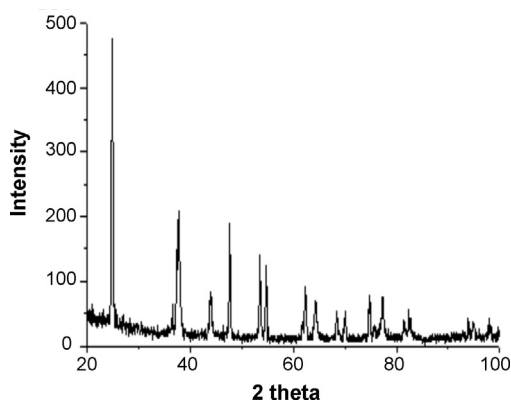


Fig. 8. XRD pattern of Au/TiO₂(P-25) synthesized by photodeposition method.

3.2. Characterization of Au/TiO₂(P-25)

3.2.1. XRD

XRD pattern of Au/TiO₂(P-25)/(4%w/w) nanocomposite synthesized by PD method is shown in Fig. 8. The Au peaks can be indexed at 2θ value 38.2°, 44.5°, 64.5°, 77.5°, 81.8°, 98.2° in addition to the titania peaks. This clearly indicates that the structural integrity of titania has been retained even after photodeposition of Au.

3.2.2. Particle size

The particle size of commercial anatase (TiO₂(anatase)) ranges from 0.1 μ m to 0.2 μ m with surface area about 13 m² g⁻¹, the anatase prepared by aerogel method (TiO₂(aerogel)) has nanosized particles ranging between 10 nm and 15 nm with high surface area of 102 m² g⁻¹. However, (TiO₂(P-25)) is nanosized with particle size of 16 nm and surface area of about 51 m² g⁻¹. Amongst all the three types of TiO₂ (TiO₂(P-25)) has a moderate particle size and high surface area.

3.2.3. UV-visible DRS

UV-visible diffused reflectance spectra of Au/TiO₂(P-25)/(4%w/w) along with bare TiO₂(P-25) is as shown in Fig. 9. In case of TiO₂(P-25), the absorption maxima is located near UV region that is 385 nm. However, in case of Au/TiO₂(P-25)/(4%w/w) nanocomposite a prominent plasmon around 550 nm was observed revealing the formation of plasmonic gold nanoparticles onto TiO₂ surface. This illustrates the presence of strong surface plasmon resonance (SPR) effect in the synthesized nanocomposite.

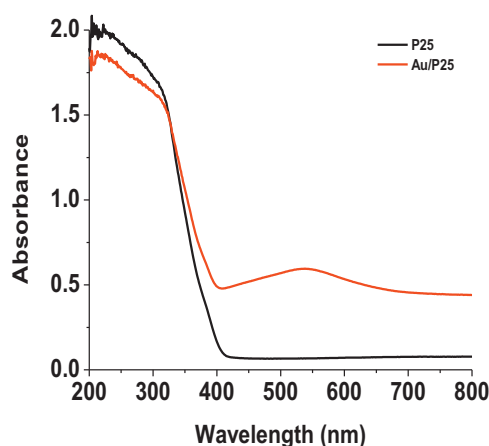


Fig. 9. UV-visible DRS spectra for TiO₂(P-25) and Au/TiO₂(P-25) composite by photodeposition method.

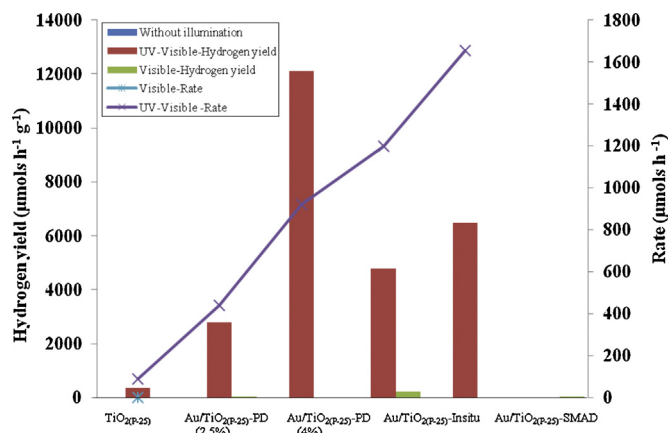


Fig. 10. Effect of synthesis route on photoactivity of Au/TiO₂(P-25) (SMAD and PD). (water:ethanol = 322:18, photocatalyst dose = 150 mg for PD and 250 mg for other photocatalysts, time duration = 5 h).

3.2.4. Transmission electron microscopy (TEM)

Transmission electron microscopic image of Au/TiO₂(P-25)/(4%w/w) is shown in Fig. 2b. Spherical and hemispherical gold nanoparticles are dispersed onto the TiO₂ matrix with particle size varying from 8 nm to 70 nm.

3.3. Comparison of SMAD and photodeposition method

In order to illustrate the effect of mode of synthesis on the activity of Au/TiO₂ nanocomposite two methods including PD method and SMAD [30] were used. The amount of hydrogen generated using PD and SMAD method is given in Fig. 10. The higher hydrogen evolution rate of Au/TiO₂(P-25) by SMAD (under optimized conditions; data reported elsewhere) in UV-visible show hydrogen evolution rate of 1600 μ mol h⁻¹ thus illustrating the role of AuNP as a co-catalyst/electron sink. In contrast, the heterogeneous particle size of AuNP by PD method appears to be detrimental with comparatively lower hydrogen evolution rate of 920 μ mol h⁻¹. However, when normalized in terms of amount of photocatalyst dose, Au/TiO₂(P-25) synthesized by PD method performs as good as Au/TiO₂(P-25) by SMAD method. Under visible light illumination Au nanocomposite by PD seems to be performing better with an enhancement by a factor about 4.7.

Thus PD method appears to be most suitable when matrix is semiconductor because in this method semiconductor (TiO₂) is excited with irradiation of suitable light wavelength to generate photoexcited electrons and holes. These photogenerated electrons reduce gold tetrachloride into metallic gold which gets deposited simultaneously on the surface of TiO₂. Ethanol which is being used as hole scavenger minimizes the electron-hole recombination reaction of TiO₂ and directs the reaction in forward direction. Au and TiO₂ are in direct contact in SMAD and PD method, which has beneficial effect on SPR. The probable reason for lower activity in visible range for Au/TiO₂ by SMAD method may be due to smaller particle size of Au-NP which is functioning very effectively as a co-catalyst and has lesser ability to harvest visible light. In addition, it is possible that in case of SMAD method there is higher fraction of mechanical mixture of AuNP and TiO₂ compared to PD with consequent effect of enhanced activity in UV-visible but lower activity in visible range which is subject to SPR effect due to direct contact of AuNPs and TiO₂.

Fig. 11 shows the bright field TEM images of (a) Au/TiO₂(P-25) in situ (b) Au/TiO₂(P-25)-PD and (c) Au/TiO₂(P-25)-SMAD. From the TEM images it is clear that gold nanoparticles have heterogeneous particle size in case of PD route as compared to in situ and SMAD method. This strengthens the above observations.

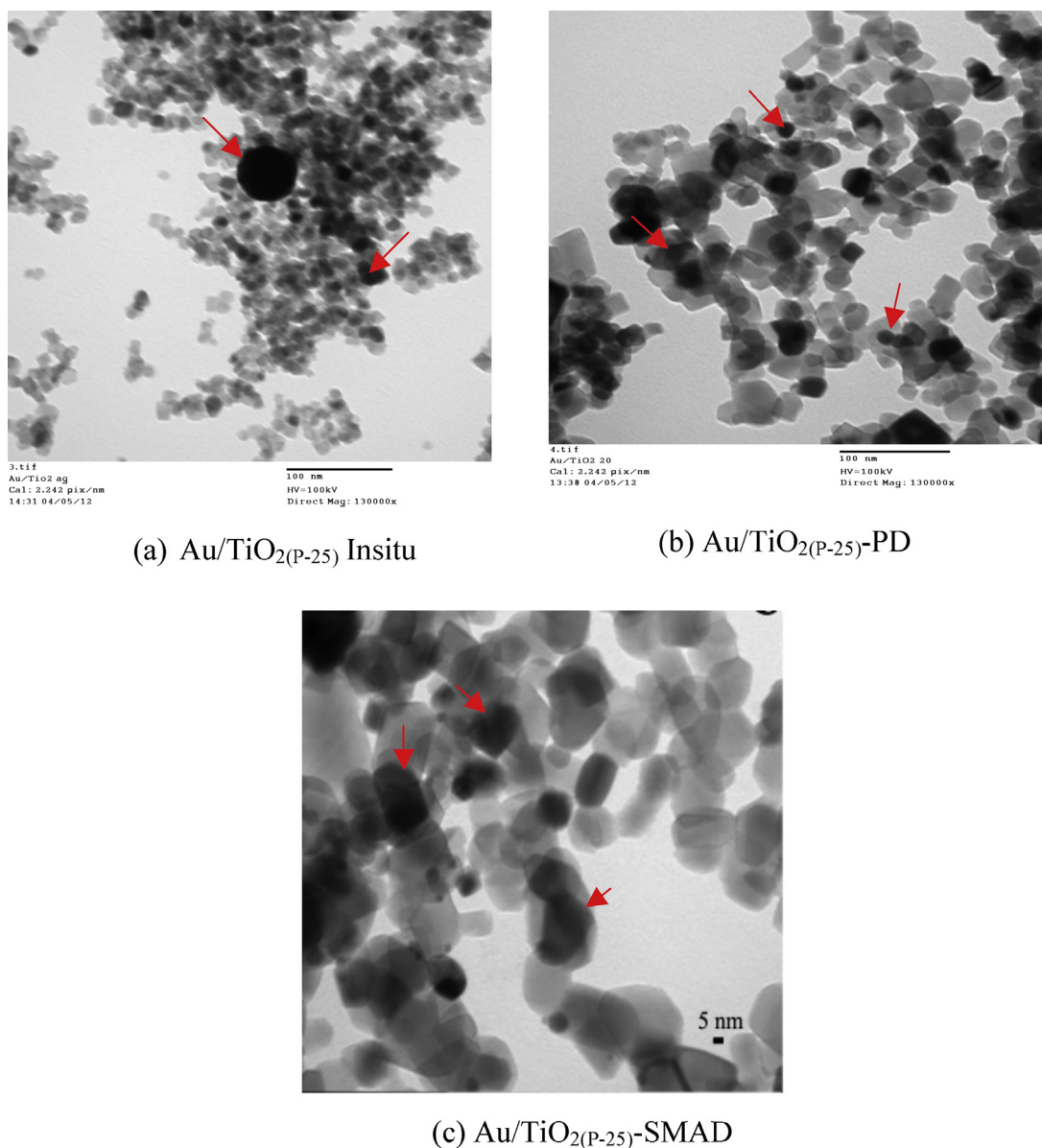


Fig. 11. Bright field TEM images of (a) Au/TiO₂(P-25) in situ and (b) Au/TiO₂(P-25)-PD and (c) Au/TiO₂(P-25)-SMAD.

3.4. Mechanistic aspects

3.4.1. Mechanism for Au/TiO₂ under UV-visible light illumination

Catalytic activity of gold nanoparticles is mainly based on its dispersion on support matrix and its particle size. The hypothesis emerging from above discussion is that Au nanoparticles are possibly playing dual role as light harvesters and injecting electrons to TiO₂ as well as acting as co-catalyst site for hydrogen generation.

UV-visible light illumination (Scheme-I):

- 1) Illumination with UV-visible light of the semiconductor TiO₂, results in photoexcitation of valence band electron to conduction band with holes at valence band.
- 2) Fermi energy level of Au nanoparticles is lower ($E_F = +0.45$ V vs NHE at pH 7 for bulk Au) that the conduction band energy level of TiO₂ ($E_{CB} = -0.5$ V vs NHE at pH 7) so these excited electrons move towards the metal thus preventing electron-hole recombination reactions.

- 3) Au nanoparticles acts as electron buffer and provides catalytic site for hydrogen generation i.e. H⁺ ions are reduced to hydrogen at Au surface by the electrons.
- 4) Holes at valence band are quenched by sacrificial electron donor i.e. ethanol. (Fig. 12a).

Visible light illumination (Scheme-II):

There are reports proposing mechanism for visible light induced photocatalytic hydrogen generation using Au/TiO₂ nanostructures. Based on these reports the possible rationalization for visible light activity is as follows:

- 1) The first hypothesis proposed by Seh et al. is "Excitation of the LSPR takes place under visible-light irradiation, resulting in the generation of plasmonic near field that are strongly localized close to the Au-TiO₂ interface. In this region, the surface-plasmon excitations are converted into electron-hole pairs via optical transitions between the localized electronic states in the band gap of the amorphous TiO₂. The presence of gold, being a large electron reservoir,

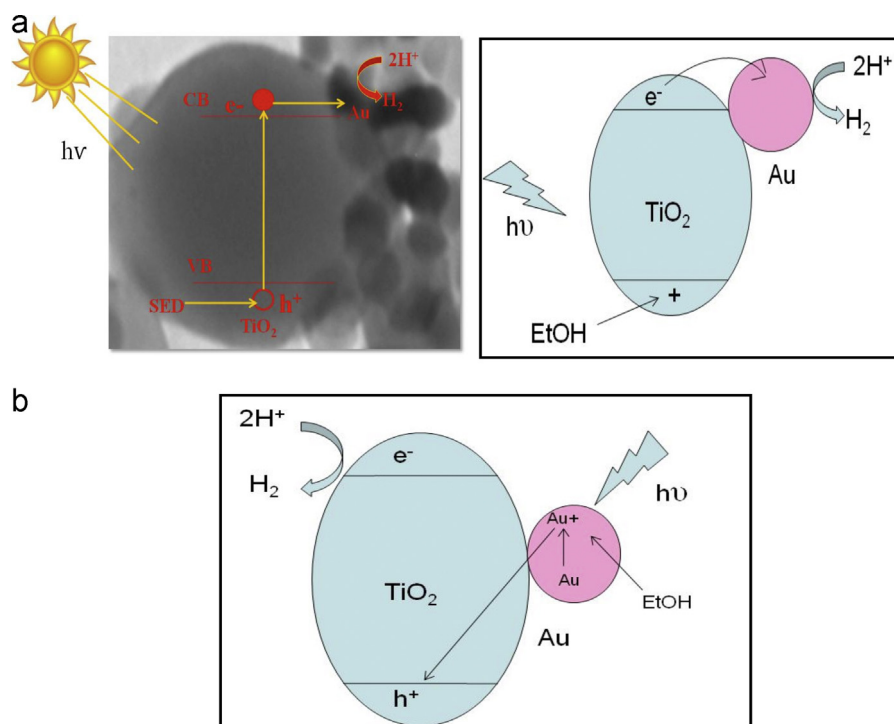


Fig. 12. (a) Possible mechanism for photoreduction by Au/TiO₂(P-25) nanocomposite (Scheme-I) and (b) possible mechanism for photoreduction by Au/TiO₂(P-25) nanocomposite.

facilitates efficient charge separation by capturing the photogenerated holes, leaving electrons in the TiO₂. The holes will subsequently be quenched by sacrificial hole trap. Because the majority of electrons are generated close to the surface without recombination, where they will reduce hydrogen ions in the aqueous solution, forming hydrogen gas" [37]. The mechanism is depicted in scheme II (Fig. 12b).

- 2) The hypothesis proposed by Gracia et al. is that "It can be, however, assumed that even if an electron hole is produced in TiO₂ conduction band, it would be replenished by the electrons of Au nanoparticles that are the less oxidizing sites of the system" [38].
- 3) The third hypothesis proposed by Tsukamoto is "Visible-light irradiation ($\lambda > 450$ nm) of gold nanoparticles loaded on a mixture of anatase/rutile TiO₂ particles (Degussa, P25) promotes efficient aerobic oxidation at room temperature. The photocatalytic activity critically depends on the catalyst architecture: Au particles with <5 nm diameter located at the interface of anatase/rutile TiO₂ particles behave as the active sites for reaction. This photocatalysis is promoted via plasmon activation of the Au particles by visible light followed by consecutive electron transfer in the Au/rutile/anatase contact site. The activated Au particles transfer their conduction electrons to rutile and then to adjacent anatase TiO₂" [36].
- 4) The fourth hypothesis proposed by Silva et al. says that "It has been determined that, due to the gold/titania interfacial contact, the conduction band of the semiconductor undergoes shift towards more negative potentials, the energy level being bent at the interface of titania by the influence of gold. Thus, the charge distribution between the gold nanoparticles and the semiconductor causes a shift of the Fermi level towards more negative potentials" [39].

As mentioned above the location of Au nanoparticle is important but size of these nanoparticles is also an important parameter. Heterogeneous sized Au nanoparticles in Au/TiO₂(P-25) in the range of 8–70 nm seems to be facilitating higher hydrogen generation possibly by above mechanism. This corroborates with the findings of Kowalska [26] & Tanaka et al. [40] wherein higher photoactivity

under visible illumination by Au particles of average size 12–60 nm and 13–70 nm respectively has been reported.

4. Conclusions

Au/TiO₂ nanocomposites shows prominent zero valent Au (Au⁰) peaks along with typical TiO₂ peaks indicating the reduction of Au (III) to (Au⁰) via PD route. Characterization and experimental details strongly suggests that enhancement in the activity is due to the formation of plasmonic state of gold nanoparticles on illumination with light source. Gold nanoparticles on illumination absorb light photon greater than or equal to its excitation energy and generate resonance surface plasmon in addition to electromagnetic energy close to the metal semiconductor interface. This enhances the generation of e⁻/h⁺ pairs at this interface. These pairs are readily separable and migrate towards the surfaces to carry out respective photocatalytic reaction. This phenomenon is reflected in enhanced photocatalytic activity under UV–visible and visible light illumination. Heterogeneous particle size of AuNP suggests that AuNP with smaller particle size probably acts as co-catalysts/electron buffer and provides active site for reduction reaction with consequent enhancement in hydrogen yield under UV–visible illumination. The bigger particle size may be functioning as light harvesters. Significant enhancement has been observed under UV–visible light illumination for hydrogen generation and needs to further improvise under visible light illumination. Further work is in progress to tailor the particle size and shape of AuNP to achieve optimal SPR effect in visible light for Au/TiO₂ nanocomposite.

Acknowledgements

Financial support from the CSIR Network project NWP-56 and Department of Chemistry, Kansas State University, Manhattan, Kansas, United States is gratefully acknowledged for providing research amenities. Dr. Boyle is also greatly acknowledged for extending help during TEM. The authors Meenal Joshi and Priti

Mangrulkar would like to thank CSIR – India for providing financial assistance in the form of Senior Research Fellowship. The authors also thankfully acknowledge Director, CSIR-NEERI, Nagpur.

References

- [1] S. Linic, P. Christopher, D.B. Ingram, *Nature materials* 10 (2011) 911–921.
- [2] M.A. EL-Sayed, *Accounts of Chemical Research* 34 (4) (2001) 257–264.
- [3] T. Ahmadi, Z.L. Wang, T.C. Green, A. Henglein, M. El-Sayed, *Science* 272 (1996) 1924.
- [4] Stephan Link, A. Mostafa, El-Sayed, *Journal of Optics A: Pure and Applied Optics* 11 (2009) 114030 (pp. 6).
- [5] J. Jiang, H. Li, L. Zhang, *Chemistry A: European Journal* 18 (2012) 6360–6369.
- [6] D.B. Ingram, S. Linic, *Journal of the American Chemical Society* 133 (2011) 5202–5205.
- [7] E. Kowalska, R. Abe, B. Ohtani, *Chemical Communications* (2009) 241–243.
- [8] M. Potara, D. Maniu, S. Astilean, *Nanotechnology* 20 (2009) 315602 (pp. 7).
- [9] C.J. Murphy, T.K. Sau, A.M. Gole, C.J. Orendorff, J. Gao, L. Gou, S.E. Hunyadi, T. Li, *Journal of Physical Chemistry B* 109 (2005) 13857–13870.
- [10] S. Tsubota, D.A.H. Cunningham, Y. Bando, M. Haruta, *Studies in Surface Science and Catalysis* 91 (1995) 227–235.
- [11] M. Haruta, *Catalysis Today* 36 (1997) 153–166.
- [12] D.I. Enache, D.W. Knight, G.J. Hutchings, *Catalysis Letters* 103 (2005) 43–52.
- [13] C. Milone, R. Ingoglia, A. Pistone, G. Neri, S. Galvagno, *Catalysis Letters* 87 (2003) 201–209.
- [14] P.L. Redmond, E.C. Walter, L.E. Brus, *Journal of Physical Chemistry B* 110 (2006) 25158–25162.
- [15] I. Ojea-Jime'nez, F.M. Romero, N.G. Bastu's, V. Puentes, *Journal of Physical Chemistry C* 114 (2010) 1800–1804.
- [16] X.M. Wang, G.J. Wu, L.D. Li, N.J. Guan, *Advanced Materials Research* 148/149 (2010) 1258.
- [17] F. Moreau, G.C. Bond, *Catalysis Today* 114 (4) (2006) 362–368.
- [18] G.H. Takaoka, T. Hamano, K. Fukushima, J. Matsuo, I. Yamada, *Nuclear Instruments and Methods in Physical Research Section B* 121 (1–4) (1997) 503–506.
- [19] R. Zanella, S. Giorgio, C.R. Henry, C. Louis, *Journal of Physical Chemistry B* 106 (31) (2002) 7634–7642.
- [20] S. Hannemann, J.-D. Grunwaldt, F. Krumeich, P. Kappen, A. Baiker, *Applied Surface Science* 252 (22) (2006) 7862–7873.
- [21] S. Ivanova, C. Petit, V. Pitchon, *Applied Catalysis A* 267 (1/2) (2004) 191–201.
- [22] D. Cunningham, S. Tsubota, N. Kamijo, M. Haruta, *Research on Chemical Intermediates* 19 (1993) 1.
- [23] M. Haruta, *Catalysis Today* 36 (1997) 153.
- [24] M. Alvaro, B. Cojocar, A.A. Ismail, N. Petrea, B. Ferrer, F.A. Harraz, V.I. Parvulescu, H. Garcia, *Applied Catalysis B: Environmental* 99 (2010) 191–197.
- [25] M.V. Dozzi, L. Prati, P. Canton, E. Selli, *Physical Chemistry Chemical Physics* 11 (2009) 7171–7180.
- [26] E. Kowalska, O.O.P. Mahaney, R. Abe, B. Ohtani, *Physical Chemistry Chemical Physics* 12 (2010) 2344–2355.
- [27] Z. Liu, W. Hou, P. Pavaskar, M. Aykol, S.B. Cronin, *Nano Letters* 11 (2011) 1111–1116.
- [28] J.J. Chen, C.S. Jeffrey, P.C. Wu, D.P. Wu, Tsai, *Journal of Physical Chemistry C* 115 (2011) 210–216.
- [29] R. Kydd, K. Chiang, J. Scott, R. Amal, *Photochemistry and Photobiology Science* 6 (2007) 829–832.
- [30] (a) K.J. Klabunde, P.L. Timms, P.S. Skell, S. Ittel, *Inorganic Syntheses* 19 (1979) 59–86;
(b) K.J. Klabunde, D. Jose, C.M. Sorensen, S.S. Rayalu, K. Shrestha, *International Journal of Photoenergy* (2013).
- [31] Y. Kuo, C.D. Frye, M. Ikenberry, K.J. Klabunde, *Catalysis Today* 199 (2013) 15–23.
- [32] K.L. McGilvray, M.R. Decan, D. Wang, J.C. Scaiano, *Journal of the American Chemical Society* 128 (2006) 15980–15981.
- [33] E. Kowalska, S. Rau, B. Ohtani, *Journal of Nanotechnology* (2012) 11 (article ID 361853).
- [34] M. Takeuchi, K. Tsujimaru, K. Sakamoto, M. Matsuoka, H. Yamashita, M. Anpo, *Research on Chemical Intermediates* 29 (6) (2003) 619–629.
- [35] Sclafani, J.M. Herrmann, *Journal of Physical Chemistry* 100 (1996) 13655–13661.
- [36] D. Tsukamoto, Y. Shiraishi, Y. Sugano, S. Ichikawa, S. Tanaka, T. Hirai, *Journal of the American Chemical Society* 134 (2012) 6309–6315.
- [37] Z.W. Seh, S. Liu, M. Low, S.Y. Zhang, Z. Liu, A. Mlayah, M.Y. Han, *Advanced Materials* 24 (2012) 2310–2314.
- [38] A. Primo, A. Corma, H. Garcia, *Physical Chemistry Chemical Physics* 13 (2011) 886–910.
- [39] C. Gomes Silva, R. Jua'rez, T. Marino, R. Molinari, H. Garcia, *Journal of the American Chemical Society* 133 (2011) 595–602.
- [40] A. Tanaka, K. Hashimoto, H. Kominami, *Chemical Communications* 47 (2011) 10446–10448.